**Proceedings of the ASME/BATH 2015 Symposium on Fluid Power & Motion Control**
**FPMC2015**
**October 12-14, 2015, Chicago, Illinois, United States**

**FPMC2015-9532**

# EXPERIMENTAL STUDY OF THE INFLUENCE OF VALVE TIMING ON HYDRAULIC MOTOR EFFICIENCY

**Hao Tian**
Department of Mechanical Engineering
University of Minnesota
Minneapolis, MN, USA 55455
tianx156@umn.edu

**James D. Van de Ven**
Assistant Professor
Department of Mechanical Engineering
University of Minnesota
Minneapolis, MN, USA 55455
vandeven@umn.edu

## ABSTRACT

The timing of the valves of a hydraulic motor plays an important role in determining the throttling energy. To reduce this dominating energy loss, the timing of the valves must allow the fluid in the chamber to be precompressed and decompressed such that there is minimal pressure differential across the transitioning valve. The optimal valve timing to achieve precompression and decompression is a function of the motor displacement, angular velocity, pressure, and air content of the fluid, thus to achieve high efficiency at all conditions, active valve timing is required. The valves in most hydraulic motor architectures are mechanically timed to the piston displacement, rendering it impossible to change the valve timing as a function of operating conditions. This paper presents one novel valve architecture that allows for such processes: a rotary valve that is controlled independently of the piston displacement, enabling active timing control. To validate the concept and test the motor valve at fixed timing and fixed displacement conditions, a prototype valve was installed on a single cylinder 3.5 cc/rev slider-crank piston motor. The nominal timing of the valve was optimized for operation for a pressure of 7 MPa, 2% entrained air by volume, and an angular velocity between 10 and 30 Hz. A model, including the pressure dynamics, leakage, compressibility, check valve dynamics, and geometry dependent parameters is developed, simulated, and compared to the experiment. The experimental system includes instrumentation for measuring the inlet and outlet flow rates, piston position, and pressure in the inlet, outlet, and cylinder. A comparison between the model and experimental data shows good agreement and demonstrate the large impact of valve timing on efficiency.

## 1 INTRODUCTION

The timing of the inlet and outlet valves play an important role in the efficiency of a hydraulic motor. Similar to how variable valve timing has been an important enabling technology for highly efficient internal combustion engines, it is believed that actively controlling the timing of a hydraulic motor can deliver similar efficiency improvements. Studies have found that the precompression and decompression of the fluid inside the piston chamber significantly improve efficiency [1-4]. Decompression is defined as the expansion of the fluid in the cylinder when the piston is just beginning to move away from top dead center (TDC) with both valves closed. Precompression is defined as the compression of the fluid in the cylinder when the piston is just beginning to move away from bottom dead center (BDC) with both valves closed.

Precompression and decompression reduce the pressure difference across the opening valve, decreasing the throttling energy loss. Martin et al. pointed out the importance of 'ideal timing' for axial piston pumps, where both the intake and the delivery valves delay to allow decompression and precompression [1]. Edge discussed the benefits and limitations of simply advancing or delaying the port plate for better compression or expansion [2]. Manring designed an efficient port plate for axial piston pumps with delayed valve openings to allow precompression or decompression of the cylinder volume [3]. Seeniraj et al. used the software CASPAR to obtain an optimized valve timing to minimize flow ripples and to increase volumetric efficiency by taking decompression and precompression into account [4]. While these studies focused on pumps, the same concepts apply to motors. A significant challenge of achieving optimal precompression and decompression in practice is that the optimal valve timing is a

 

function of the pump/motor displacement, angular velocity, pressure, and the fluid compressibility.

To achieve the desired precompression and decompression processes for a variety of operating conditions, active valves are required, with options including movable port plates, solenoid valves, and custom designs. While port plates, as commonly found in axial piston and bent axis pumps/motors, are typically fixed, previous work has explored making them variable by swapping multiple sets of port plates [5]. Alternatively, off-the-shelf solenoid valves have been widely used to control the timing in digital pumps. Rannow et al. experimentally studied the possibility of using commercial solenoid valve to emulate an on-off valve to create a variable displacement pump [6]. In recent years, Holland [7] and Merill [8] both present digital pumps based on solenoid valves. Artemis Intelligent Power has commercialized the digital displacement technology using digital valve control [9]. Wadsley also demonstrated digital valve enabled high efficiency pumps under development at Sauer-Danfoss [10].

In addition to solenoid valves, researchers have developed a number of custom valve architectures for switch-mode circuits that can be used to guide development of active motor valves. One popular approach is rotary valve. Royston et al. studied a rotary pneumatic valve with a concentric two-tier cylinder design [11]. Their continuous uni-directional valve rotation eliminated inertial forces, but the complex multiple sealing surfaces created leakage challenges. Katz et al. developed a two-tier continuously rotating disc style valve with axial flow paths [12]. Poor experimental efficiency was observed due to component alignment difficulties, unpredicted leakage, and bearing preload friction. Tu et al. presented a cylindrical rotary spool valve with rhombus shaped orifices with the capability of continuously varying the duty ratio and being propelled by the working fluid [13]. The leakage due to the complex flow paths limits the maximum volumetric efficiency of the valve to below 75%.

There are benefits and tradeoffs for each kind of the active valve. For the port plates, the valve timing has excellent reliability and repeatability, but requires either disassembling the motor to change the valve timing or complex adjustment mechanisms. Commercially available solenoid valves suffer from slow response times. A promising valve option for active valve control of a motor is a continuously rotating rotary valve due to the fast transition time and variable valve timing capability, provided the leakage issue and the actuation problems are solved.

In this paper, a novel rotary valve architecture for hydraulic piston motors is introduced that uses a single-stage uni-directional rotary structure with adjustable radial hydrodynamic clearance. As shown in Figure 1, the three-way three-position valve features a cylindrical rotor and a mating sleeve, which form the hydrodynamic surface. The continuously rotating rotor spool alternatively connects the cylinder (C) port to either the pressure (P) or the tank (T) port. There are two pairs of ports, such that the valve is switched on and off twice per revolution. When the valve sleeve is unwrapped onto a plane, the ports have a rectangular shape allowing for a linear and fast transition. The rotor can be driven actively by a servo motor, stepper motor, or passively by the motor shaft. When driven actively, the valve enables adjustment of the duration of the valve transitions to minimize the throttling loss. The hydrodynamic surface between the valve rotor and the inside of the sleeve have a 2-degree taper. By adjusting the axial position of the rotor relative to the sleeve through shims, the radial clearance of the valve can be accurately set. The well controlled radial clearance also manages the viscous friction and leakage trade-off.

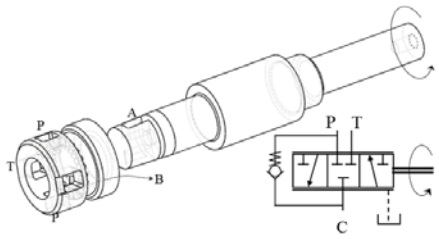


*Figure 1. The active rotary valve and symbol.*

The rotary valve angular position must be actively controlled to achieve the desired valve timing. As shown in Figure 2, the rotary valve is driven by a computer operated stepper motor with position feedback. The benefit of having a 'steer-by-wire' valve or valve timing completely decoupled from the crank shaft position is that now one extra degree of freedom is gained for valve timing manipulation.

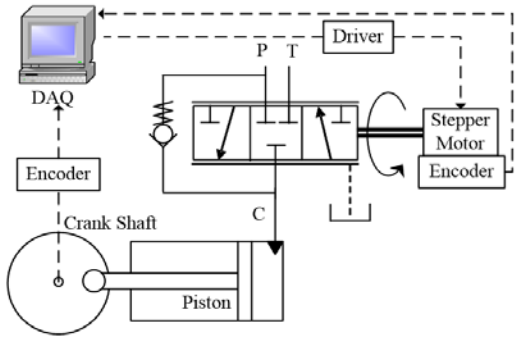


*Figure 2. The 'steer-by-wire' rotary hydro motor valve concept.*

The primary objective of this paper is to computationally and experimentally explore the influence of valve timing on hydraulic motor efficiency. The secondary objective is to investigate the feasibility of the proposed active rotary valve concept. In this paper, the rotary valve will only be used in a fixed timing mode where the control circuit synchronizes the valve to the motor shaft rotation. Actively varying the valve timing will be explored in future work. The detailed mathematical model for the motor valve system is derived in section 2. The experimental setup and test procedure are explained in section 3. Experimental results are presented in section 4, followed by a discussion and concluding remarks in sections 5 and 6 respectively.

## 2 MATHEMATICAL MODEL

**2.1 Governing Equation of Cylinder Pressure.** Figure 3 shows the control volume (CV) and the variables for the motor valve model. The lumped pressure inside the piston cylinder is a function of piston displacement and the flow through the control surfaces, described as:

$$\dot{p} = -\frac{\beta_e}{V}\left(\dot{V} - q_i - q_o - q_{lk} - q_{ck}\right) \tag{1}$$

where $\beta_e$ is the effective bulk modulus, $\dot{p}$ is the time derivative of the cylinder pressure, $\dot{V}$ is the time derivative of the piston volume with respect to time, $q_i$ is the flow rate in from the pressure port, $q_o$ is the flow rate out to the tank port, $q_{lk}$ is the leakage flow rate through the valve, and $q_{ck}$ is the flow rate through the bypass check valve.

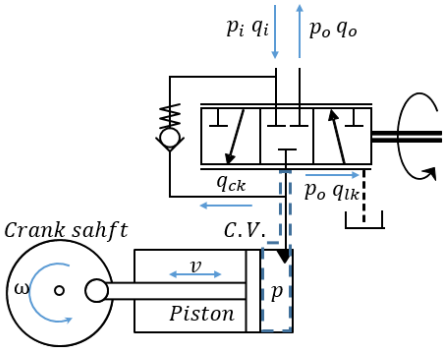


*Figure 3. The control volume and the variables of the motor valve model.*

### 2.2 Fluid Model

*2.2.1 Bulk Modulus.* The effective bulk modulus for oil with entrained air is modeled using the Cho et al. relationship [14]:

$$\beta_e = \frac{R + \left(\frac{p}{p_0} + 1\right)^{\frac{1}{\gamma}}}{\frac{R}{\gamma}\frac{\beta_0}{p + p_0} + \left(\frac{p}{p_0} + 1\right)^{\frac{1}{\gamma}}}\beta_0 \tag{2}$$

where $p_0$ is the atmospheric pressure, $\gamma$ is the heat capacity ratio, $R$ is the volumetric fraction of entrained air at $p_0$ pressure, and $\beta_0$ is the bulk modulus of oil without air.

The assumptions made in the model are a constant mass ratio between the gas and liquid phase, no vaporization, no dissolving of the entrained air, and no release of the dissolved air.

*2.2.2 Density.* The density of the hydraulic oil inside the CV is derived from the bulk modulus definition and described as:

$$\rho = \rho_0\left(1 + \frac{p - p_0}{\beta_e}\right) \tag{3}$$

### 2.3 Flow Model

*2.3.1 Geometry-dependent Valve Orifice Flow Model.* The volumetric flow rate through the valve is defined using orifice flow equation, described as:

$$q_{i,o} = c_q A(\theta)\sqrt{2\Delta p/\rho} \tag{4}$$

where the discharge coefficient, $c_q$, is found experimentally. The geometry-dependent parameter, the instantaneous orifice area $A(\theta)$, can be found from the relative position between the unwrapped inner sleeve and the valve rotor port, as shown in Figure 4, and is described as:

$$A(\theta) = \frac{l_p w}{2\pi} \cdot \begin{cases} 0 & \theta_{te} + \theta_r \le \theta < \theta_{ps} - \theta_r \\ \theta + \theta_r - \theta_{ps} & \theta_{ps} - \theta_r \le \theta < \theta_{ps} + \theta_r \\ \theta_r & \theta_{ps} + \theta_r \le \theta < \theta_{pe} - \theta_r \\ \theta_{pe} - \theta & \theta_{pe} - \theta_r \le \theta < \theta_{pe} + \theta_r \\ 0 & \theta_{pe} + \theta_r \le \theta < \theta_{ts} - \theta_r \\ \theta + \theta_r - \theta_{ts} & \theta_{ts} - \theta_r \le \theta < \theta_{ts} + \theta_r \\ \theta_r & \theta_{ts} + \theta_r \le \theta < \theta_{te} - \theta_r \\ \theta_{te} - \theta & \theta_{te} - \theta_r \le \theta < \theta_{te} + \theta_r \end{cases} \tag{5}$$

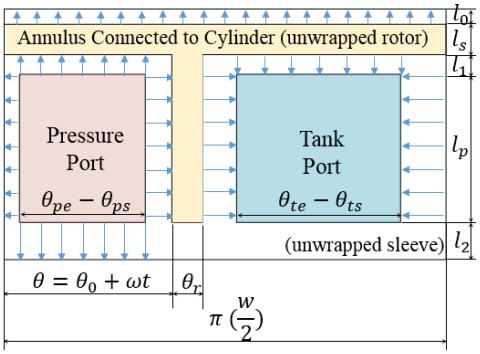


*Figure 4. The unwrapped valve geometry at given angle.*

*2.3.2 Geometry-dependent Leakage Model.* The volumetric leakage flow rate is modeled as parallel plate flow:

$$q_{lk} = \frac{\Delta p B h^3}{12\mu L} \tag{6}$$

where $\Delta p$ is the pressure differential across the leakage path, $B$ and $L$ are the leakage path width and length respectively, $\mu$ is the dynamic viscosity, and $h$ is the hydrodynamic clearance.

The relative position between the cylinder port and the P/T ports changes as the rotor angle, $\theta$, changes. In the calculation for leakage when the valve is set to be fully closed, $\theta$ is fixed and set to be in between the P and T ports. In the cylinder pressure dynamic simulation, $\theta$ is updated at each calculating step based on angular velocity, resulting different leakage paths. A transitional zone is set by the port edges where orifice equation is used when the predicted $q_{lk}$ is greater than that of the orifice

flow. The geometric parameters for calculating the leakage are presented in Table 1.

*Table 1. The geometry parameters for calculating leakage.*

| Variable | Description | Value | Unit |
|---|---|---|---|
| $\theta_r$ | System port angle | 0.29 | *rad* |
| $\theta_{pe} - \theta_{ps}$ | Pressure port width | 1.39 | *rad* |
| $\theta_{te} - \theta_{ts}$ | Tank port width | 1.44 | *rad* |
| $w$ | Unwrapped sleeve width | 45.93 | *mm* |
| $l_0$ | System port to upper edge length | 3.90 | *mm* |
| $l_1$ | System to pressure/tank length | 1.40 | *mm* |
| $l_2$ | Port to lower edge length | 2.62 | *mm* |
| $l_s$ | System port width | 1.60 | *mm* |
| $l_p$ | Pressure/tank port width | 6.37 | *mm* |
| $h$ | Parallel plate distance | 11 | $\mu m$ |

*2.3.3 By-pass Check Valve Model.* A check valve is used to prevent excessive pressure in the piston by returning the fluid to the high pressure rail. As shown in Figure 5, a simple check valve dynamic model, based on the dynamics of a spring-mass-damper system, is used to predicted the axial displacement of the poppet and thus provide the actual check valve open area $A_{ck}$. The instantaneous volumetric flow rate is defined using the orifice flow equation:

$$q_{ck} = c_q A_{ck} \sqrt{2(p - p_i)/\rho} \tag{7}$$

where the open area of the check valve $A_{ck}$, and the spring-mass damper dynamics are described by:

$$A_{ck} = 2\pi r d \cos\alpha \tag{8}$$

$$m\ddot{d} + c\dot{d} + kd = \Delta p \pi r_p^2 \tag{9}$$

The coefficients $m$ and $k$ are measured from the off-the-shelf check valve. The oil damping coefficient, $c$, is determined simulating the check valve dynamics alone and tuning the coefficient such that the poppet oscillation duration is less than half of the cycle time. Only pressure force is considered.

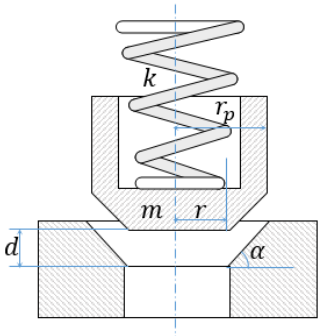


*Figure 5. Check valve geometry.*

**2.4 Energy and Piston Efficiency Model.** To decouple the influence of un-modeled motor kinematics and make this study more general, 'piston efficiency' for hydraulic motor is defined as the ratio between the output piston boundary work and input fluid work. The overall input fluid energy $w_{in}$ for a given multi-cycle period between $t_1$ and $t_2$ is defined as the summation of the integral of the input fluid work and the integral of the compressible potential energy, as shown in Eqn.(10).

$$w_{in} = p_i \int_{t_1}^{t_2} q_i \, d\tau + \frac{(t_2 - t_1)}{t_c} \int_{TDC}^{BDC} pdV \,|_{p>p_0} \tag{10}$$

where $p_i$ and $q_i$ are pressure and flow rate probed at the inlet of the motor. The input fluid work term $p_i \int_{t_1}^{t_2} q_i \, d\tau$ represents the boundary work done by the moving pressure column.

The compressible potential energy term $\int_{TDC}^{BDC} pdV$ in Eqn.(10) is the compressible potential energy per cycle, and is usually neglected in the traditional motor model. Neglecting this term is reasonable if the stiffness of the fluid is high. This assumption is no longer be valid when significant amount of entrained air is present. If the compressible energy is not accounted for in this case, the overall fluid input work will be under-predicted. For motors with fixed valve timing, the compressible potential energy is often dissipated by throttling across the opening tank valve near bottom dead center.

The output boundary work at the piston is defined as:

$$w_{out} = \int_{t_1}^{t_2} (pA_p - p_0 A_r) v d\tau|_{v>0} \tag{11}$$

where $A_p$ and $A_r$ are the respective area of the piston side and rod side, $v$ is piston velocity. Note that this definition neglects piston friction and inertial effects. The piston efficiency is then defined as:

$$\eta_p = \frac{w_{out}}{w_{in}} = \frac{\int_{t_1}^{t_2} (pA_p - p_0 A_r)\, v d\tau|_{v>0}}{p_i \int_{t_1}^{t_2} q_i \, d\tau + \frac{(t_2 - t_1)}{t_c} \int_{TDC}^{BDC} pdV \,|_{p>p_0}} \tag{12}$$

## 3 EXPERIMENTAL STUDY

Two experiments are presented in this paper: 1) characterizing the custom rotary valve and 2) validating the pressure dynamics model developed in section 2. The valve is characterized in two ways, first by measuring the pressure drop versus flow rate at in the fully open state and then measuring the leakage across the ports at the fully closed state. To validate the pressure dynamics model, the active rotary valve is installed on a commercial crank-slider pump to allow it to operate as a single piston fixed-displacement hydraulic motor. The motor is instrumented such that pressure transients, energy distribution, and the piston efficiency can be found.

Two different setups were used for the valve characterization and the valve-motor experiments. Figure 6 shows the test circuit designed to map the flow and volumetric

performance of the valve as a standalone component. The circuit consists of a hydraulic power supply, a flow meter, and the rotary valve with pressure transducers installed at the intake and cylinder ports. In experiment, the valve rotor is turned to the desired position, i.e. closed or open fully, while the pressure of the hydraulic power supply is set to pressure increments between 10 bar and 70 bar. The leakage experiments were run at four different radial clearances, set with the axial position of the valve rotor in the tapered sleeve.

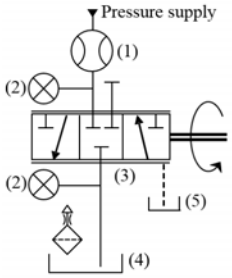


*Figure 6. The standalone test circuit. (1-Gear flow meter; 2-pressure sensors; 3-rotary valve; 4-reservoir; 5-measuring flask)*

Figure 7 shows the hydraulic circuit designed to evaluate the pressure dynamics of the hydraulic motor. Figure 8 shows a picture of the motor test bed. The hydraulic motor is constructed from a commercial crank-slider pump, where the rotary valve is connected to one of the three cylinders, while the other two pistons are removed. The high pressure branch of the hydraulic circuit consists of a hydraulic power supply, a gear flow meter, and an accumulator mounted next to the rotary valve to minimize the pressure ripple. The low pressure branch includes an accumulator and a Coriolis flow meter. During power stroke, the high pressure fluid enters the piston-cylinder through the rotary valve and extends the single cylinder from TDC to BDC. During the exhaust stroke, the fluid is pushed out of the cylinder through the rotary valve to the low pressure branch, where an accumulator minimizes the pressure ripple before the fluid travels back to tank. As a safety device, a check valve with a cracking pressure of 5 psi is mounted between the piston-cylinder and the high-pressure branch. Pressure transducers are used to measure the pressure at the high pressure and tank ports of the valve and in the piston-cylinder. A complete list of apparatus can be found in Table 2.

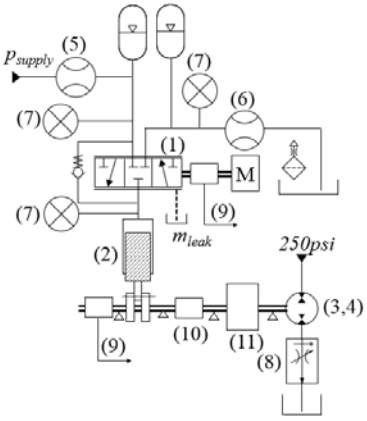


*Figure 7. Motor experiment hydraulic circuit. (1-rotary valve; 2-crank-slider pump; 3,4-gerotor motor; 5-gear meter; 6-coriolis meter; 7- pressure sensors; 8-pressure compensated flow control valve; 9-rotory encoders; 10-torque sensor; 11-flywheel.)*

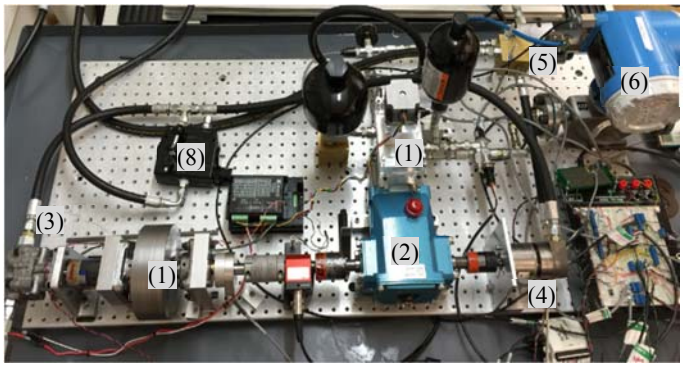


*Figure 8. Photo of the test bed. (1-rotary valve; 2-crank-slider pump; 3,4-gerotor motor; 5-gear meter; 6-coriolis meter; 8-pressure compensated flow control valve.)*

*Table 2. List of experimental apparatus.*

| No. | Part Name | Part No. |
|---|---|---|
| 1 | 3/3 way rotary valve | In-house design |
| 2 | CAT plunger pump | 5CP3120 |
| 3 | Geroter pump/motor | MGG20010 |
| 4 | Geroter pump/motor | C-L129-0002 |
| 5 | Gear flow meter | JVA20KG25NPT |
| 6 | Coriolis flow meter | Promass 80 |
| 7 | Pressure transducer | MLH03KPSI01A |
| 8 | Flow Control Valve | RDRS137-08 |
| 9 | Master DAQ | PCI-6251 |
| 10 | Secondary DAQ | USB-6009 |
| 11 | Stepper motor | 57BYGH310 |
| 12 | Stepper motor driver | CWD556 |
| 13 | Flywheel | In-house design |
| 14 | Hydraulic fluid | DTE 25 |

The angle of the motor crankshaft and the valve rotor are measured with quadrature rotary encoders. The synchronization between the crankshaft and the valve rotor is realized through position feedback control using a PI controller. The valve rotor and sleeve were previously designed to create valve timing for a fixed-displacement single-cylinder hydraulic motor, running at 7 MPa, 2% entrained air by volume, and an angular velocity between 10 and 30 Hz [15]. This optimal valve timing and the actual valve timing as machined are presented in Figure 9. Significant discrepancies are found around 10, 90, 175, and 275 degree crank shaft angles. While more accurate timing is preferred, these mismatches provide a good case study to help understand the importance of valve timing, and help validate the model.

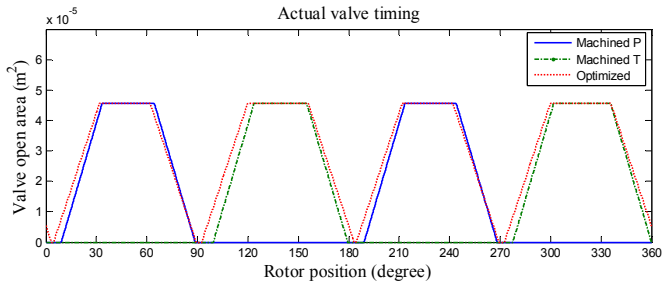


*Figure 9. Designed and actual valve timing profiles.*

## 4 RESULTS AND MODEL VALIDATION

**4.1 Valve Characterization.** The results of the pressure-drop versus flow rate experiment across the fully-open valve are presented in Figure 10. By performing a least-squares fit between the data and the orifice equation, the valve discharge coefficient $c_q A$ is found to be 1.15e$^{-5}$m$^2$.

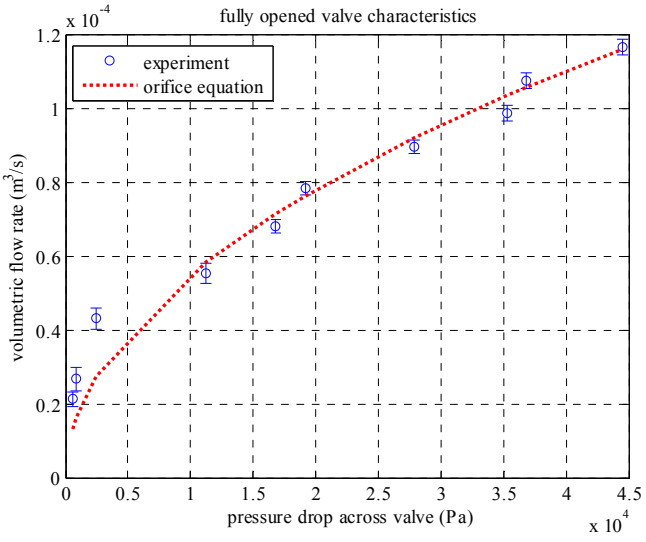


*Figure 10. The flow rate and pressure drop across the valve.*

The experiment evaluating the leakage across the fully-closed valve was performed at four radial clearances from 2.7 $\mu$m to 11.5 $\mu$m. In Figure 11, the measured leakage rate is compared to the geometry-dependent leakage model described in Sec. 2.3.2. The highest leakage flow rate recorded in the experiment is less than 1 cc per second, much smaller than the nominal motor flow rate of 52.5cc per second at 15Hz.

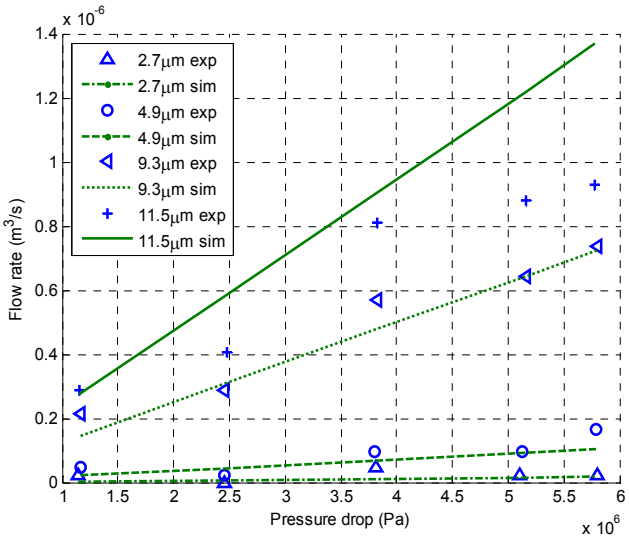


*Figure 11. The leakage flow rate at different pressure differentials.*

**4.2 Cylinder Pressure Transients.** The pressure transients in the piston cylinder of the motor are a good indicator of model accuracy. The cylinder pressure dynamics model described in Sec. 2 is validated by comparing to the experiment profiles. The model is simulated using Newton-Eulerian solver, the tolerance for convergence is set to be 1e$^{-5}$ Pa, the time step is set between 1e$^{-5}$ and 2e$^{-5}$ seconds. The input to the simulation is the measured valve timing profile, the supply pressure from the experiment, and the experiment duration. The volumetric fraction of air at atmospheric pressure is set to 2%. Figure 12 shows the comparison between experimental and simulation results at 30 bar 5Hz, 50bar 10Hz, and 70bar 15Hz. Note the difference in shape between the two pressure steps are due to the unique shape of each port cause by machining processes. The model is able to capture the differences between two port sets, and tracks the pressure transients reasonably well.

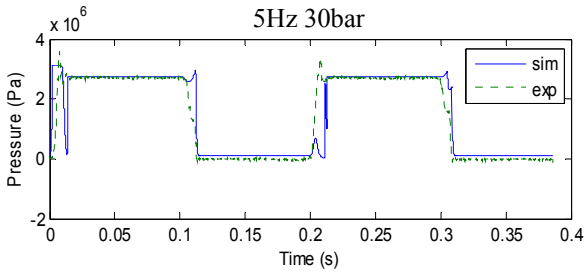

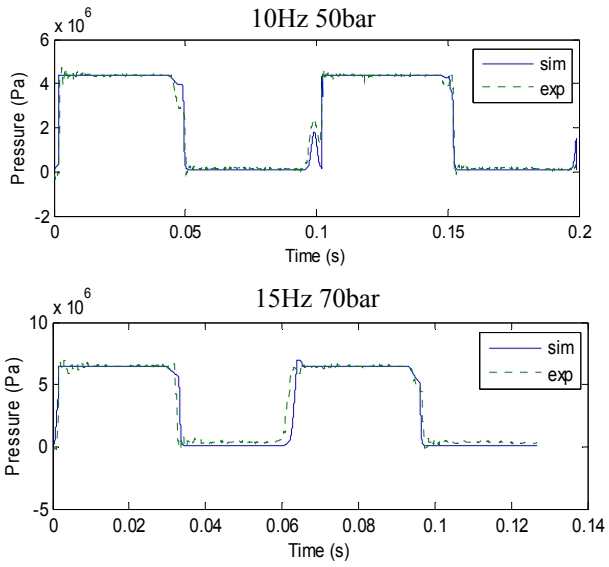


*Figure 12. Comparison between model and measured cylinder pressure profiles as pressure and rpm vary.*

**4.3 Piston Efficiency.** The input fluid work, output piston work, and piston efficiency are calculated based on Eqn. (10), (11) and (12). An industrial hydraulic power supply is used in the experiment, where large tanks and good filtration ensure a low entrained air fraction. As the compressible potential energy of the inlet fluid is small at low air fractions, it is safe to be neglected in this calculation, i.e. at 70 bar only 1.2% of the total input fluid energy is contributed by the compressible potential with 2% entrained air by volume at atmospheric pressure. Figure 13 shows the experimental motor piston efficiency versus the simulated values for a pressure range between 20 bar and 70 bar, and a rotation frequency range between 5 Hz and 15 Hz, each experimental data point is calculated from an average of at least 30 motor cycles. The average experimental piston efficiency is above 90%.

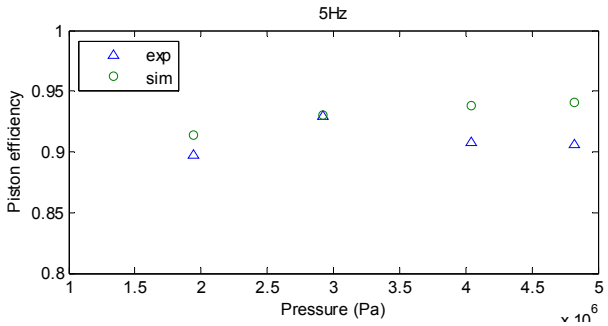


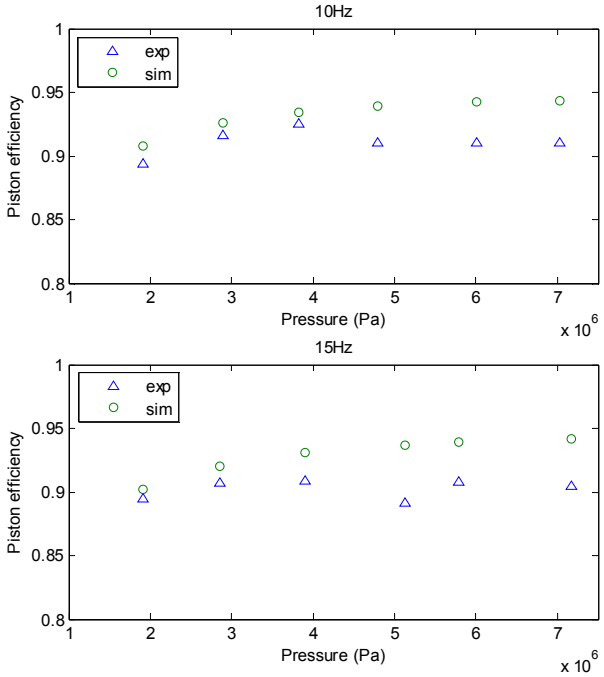


*Figure 13. Motor piston efficiency at different pressure and rpm.*

## 5 DISCUSSION

In the baseline study, the valve discharge coefficient $c_q A$ found for the fully opened case is 1.15e$^{-5}$ m$^2$. The experimental hydrodynamic clearance value was determined by placing shims of known thickness to axially shift the tapered valve rotor. Figure 11 demonstrates good consistency between model and experiment results at 2.7 $\mu m$, 4.9 $\mu m$ and 9.3$\mu m$ clearances, but over-predicts the leakage at 11.5 $\mu m$ clearance. It is believed that a higher preload stress existed with the thicker shim stack, cause the shims to deform. To test this hypothesis, a clearance of 10.5 $\mu m$ was input to the model instead of the expected 11.5 $\mu m$ clearance, generating a better match between experimental data and the model, as shown in Figure 14.

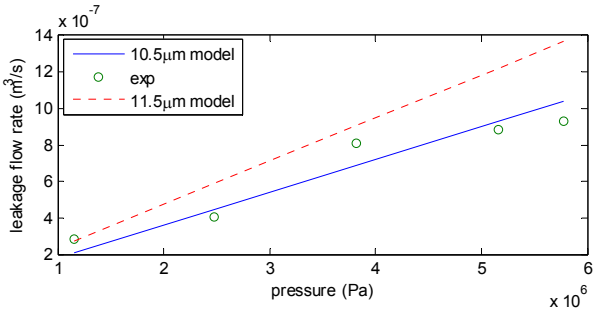


*Figure 14. Reduce the model clearance value by 1μm.*

When analyzing the motor performance, a separation of energy loss terms improves the understanding of the impact of each term on the valve performance. The dissipative terms are

isolated and individually identified. The power of throttling loss is described as:

$$\dot{w}_t = \frac{1}{t_2 - t_1}\int_{t_1}^{t_2} \Delta p q_{i,o}\, d\tau$$

The flow rate $q_{i,o}$ for calculating the throttling power is based on volumetric piston displacement from crank shaft angular position measurement. The average power is calculated from the work done for a duration between $t_1$ and $t_2$, and a cycle time of $t_c$.

The leakage power loss is described as:

$$\dot{w}_l = \frac{1}{t_2 - t_1}\int_{t_1}^{t_2} \Delta p q_{lk}\, d\tau \qquad (14)$$

where the leakage flow rate $q_{lk}$ is based on the captured leaking volume.

The viscous friction power is calculated based on the overlapping area between the valve rotor and sleeve at each valve rotor position from 0 to $2\pi$, and the measured rotor tangential velocity $v_{rt}$:

$$\dot{w}_v = \frac{1}{t_2 - t_1}\int_{t_1}^{t_2} \frac{\mu v_{rt}^2 \mathrm{w} l}{h}\, d\tau \qquad (15)$$

Finally, the compressible potential power, an input to the motor, is calculated based on an isothermal assumption:

$$\dot{w}_c = \frac{1}{t_c}\int_{TDC}^{BDC} pdV\,|_{p>p_0} \qquad (16)$$

Figure 15 shows the spectra of all the power terms at various shaft frequencies and pressures, calculated from the average of 40 cycles at the machined timing. The output power of the single cylinder motor is 39.9W at 1.9MPa and 5Hz, and 377.6W at 7.2MPa and 15Hz.

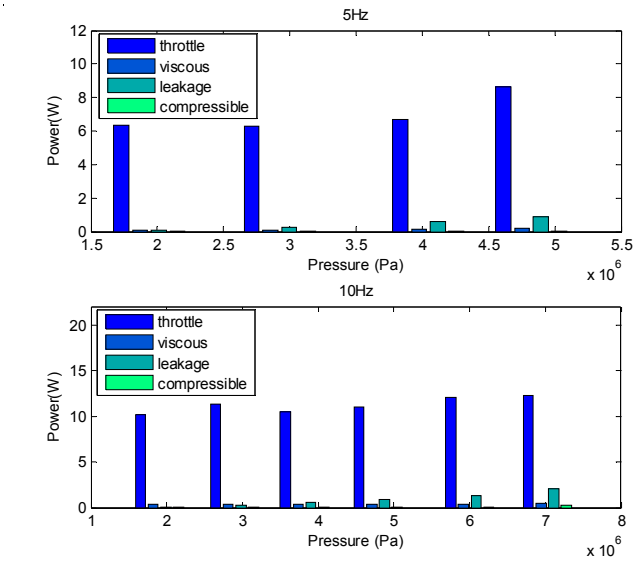


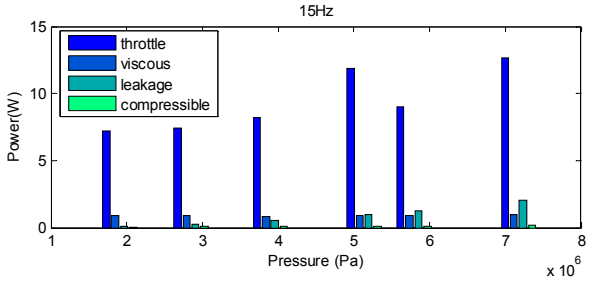


*Figure 15. Dissipative power spectra at 5, 10, and 15Hz.*

As expected, the throttling power dominates all cases, leakage and viscous friction are only a fraction of the throttling loss. Note the compressible potential power is counted as an input power. It is interesting to see the compressible potential power increases as pressure goes up, but the overall magnitude is low. However, under higher pressure and higher air content, if the valve timing deviates from the optimal, the potential energy will dissipate through throttling, resulting in heat generation and a loss of efficiency.

In Figure 13, it is noticed that the simulated piston efficiency scales with pressure. The throttling loss power and input fluid power both increase with pressure as described in Eqn.(10) and (13), but the former does at a much slower rate, as shown by the experimental data in Figure 15. Thus, when the supply pressure increases, the simulated piston efficiency goes up. However in Figure 13, experimental piston efficiency starts to deviate from the model when the pressure is greater than 4MPa. Because the experimental test bed uses a single cylinder, torque is only applied to the crankshaft for half of the cycle, causing the crank shaft speed to fluctuate. As illustrated in Figure 16, at higher pressures the increase in tracking error causes a deviation in the valve timing. The speed fluctuations increase with pressure, affecting the rotor tracking performance. A misalignment between crank shaft position and valve timing results in increased throttling loss.

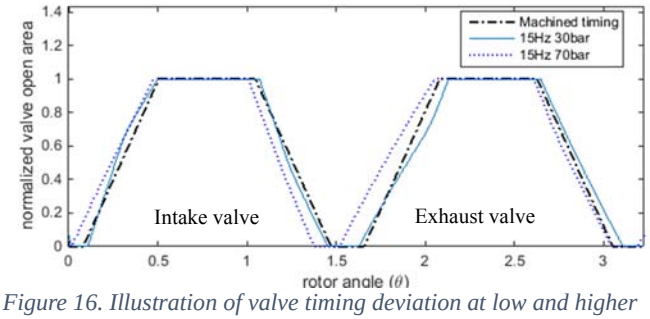


*Figure 16. Illustration of valve timing deviation at low and higher pressure.*

It is intriguing to further explore the impact of valve timing on the throttling loss. To showcase the valve timing effect, Figure 17 compares the throttling power among three different situations: the experimental system, the simulated system with the experimental valve timing, and the simulated system using the previously optimized timing at 15Hz.

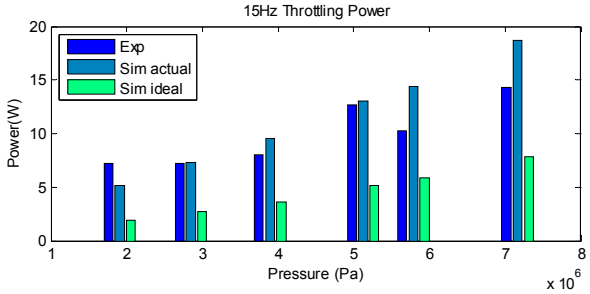


*Figure 17. Comparison among experimental and simulated throttling loss at actual or ideal valve timing.*

From Figure 17, the simulation agrees well with the experimental results for most cases. It also indicates that the valve timing has significant impact on the hydraulic motor performance. If the experiment were to use the optimal timing, the throttling loss could be reduced by 50% over the current value, and increase the piston efficiency by 5%.

To further understand the throttling loss and illustrate the impact of the valve transitional stage, Figure 18 shows a comparison between the experimentally measured throttling loss power when the valve is transitioning vs fully open at 15 Hz. A threshold is established to define the transitioning period as the port area less than 30% of the total port area. The experimental result indicates that a 0 ~ 30% valve transition to fully open only takes 24.4% of the cycle time, but actually contributes nearly half of the total throttling loss. By reducing the transition time, it is believed the piston efficiency could be further improved.

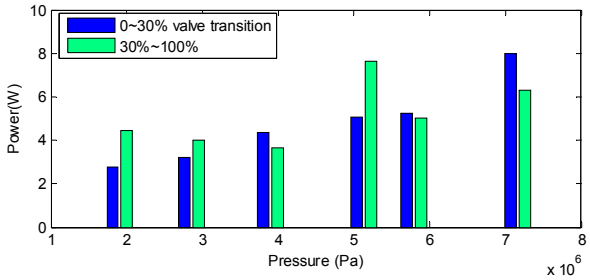


*Figure 18. Throttling power during different valve opening stages.*

## 6 CONCLUSION

The throttling loss is one of the major energy dissipative sources for positive displacement hydraulic motors. The optimal valve timing to minimize throttling energy loss is a function of the pressure, angular velocity, and the entrained air fraction. To improve motor performance, a novel active rotary valve that is potentially capable of varying the valve timing based on the operating conditions is introduced and modeled. The rotary valve was experimentally demonstrated on a single-cylinder 3.5 $cm^3$ hydraulic motor running between 5 and 15Hz. The motor was operated at different pressures and speeds, demonstrating good agreement between the model predicted and experimentally captured piston efficiency. Detailed performance analysis shows the throttling loss is the dominated energy loss term. The significance of optimal valve timing is also illustrated through a comparison between experimental and optimal timing, showing an opportunity to improve the piston efficiency by at least a 5%. Future work for this research includes: 1) developing a the control algorithm actively vary the valve timing to approach the optimal solution, and 2) studying the relationship between motor working conditions and the respective optimal valve timing profiles.

## NOMENCLATURE

| | | |
|---|---|---|
| $A$ | Instantaneous valve open area | $[m^2]$ |
| $A_{ck}$ | Open area of the check valve | $[m^2]$ |
| $A_p$ | Piston side area | $[m^2]$ |
| $A_r$ | Rode side area | $[m^2]$ |
| $\alpha$ | Poppet angle | $[^o]$ |
| $B$ | Width of the hydrodynamic surface | $[m]$ |
| $\beta_0$ | Bulk modulus of pure DTE25 | $[Pa]$ |
| $\beta_e$ | Effective bulk modulus | $[Pa]$ |
| $c$ | Oil damping coefficient | |
| $c_q$ | Discharge coefficient | |
| $d$ | Poppet displacement | $[m]$ |
| $h$ | Hydrodynamic clearance | $[m]$ |
| $k$ | Check valve spring constant | $[\frac{N}{m}]$ |
| $L$ | Length of the hydrodynamic surface | $[m^2]$ |
| $m$ | Check valve poppet mass | $[kg]$ |
| $\eta_p$ | Piston efficiency | |
| $P$ | Pressure port notation | |
| $p_i$ | Supplied pressure | $[Pa]$ |
| $p_o$ | Tank pressure | $[Pa]$ |
| $\rho$ | Density | $[\frac{kg}{m^3}]$ |
| $\rho_0$ | Density at atmospheric pressure | $[\frac{kg}{m^3}]$ |
| $q_{ck}$ | Check valve flow rate | $[\frac{m^3}{s}]$ |
| $q_{lk}$ | Leakage flow rate | $[\frac{m^3}{s}]$ |
| $q_i$ | Intake flow rate | $[\frac{m^3}{s}]$ |
| $q_o$ | Exhaust flow rate | $[\frac{m^3}{s}]$ |
| $r$ | Poppet port radius | $[m]$ |
| $r_p$ | Poppet radius | $[m]$ |
| $\gamma$ | Heat capacity ratio | |
| $R$ | Volumetric percentage of entrained air | |
| $S$ | Cylinder port notation | |
| $T$ | Tank port notation | |
| $t$ | Time | $[s]$ |
| $t_2 - t_1$ | Experimental duration | $[s]$ |
| $t_c$ | Motoring cycle time | $[s]$ |
| $\mu$ | Dynamic viscosity | $[Pa\,s]$ |
| $V$ | Piston chamber volume | $[m^3]$ |
| $v$ | Piston velocity | $[\frac{m}{s}]$ |
| $v_{rt}$ | Rotor tangential velocity | $[\frac{m}{s}]$ |
| $w$ | Work | $[J]$ |

| | | |
|---|---|---|
| $w_{in}$ | Input work | $[J]$ |
| $w_{out}$ | Output work | $[J]$ |
| $\dot{w}_c$ | Compressibility potential power | $[W]$ |
| $\dot{w}_l$ | leakage loss power | $[W]$ |
| $\dot{w}_t$ | Throttling loss power | $[W]$ |
| $\dot{w}_v$ | Viscous loss power | $[W]$ |

## ACKNOWLEDGMENTS

This work is supported by the National Science Foundation under grant number EFRI-1038294.

## REFERENCES

[1] M. M. a. R. Taylor, "Optimised port plate timing for an axial piston pump," in *5th International Fluid Power Symposium*, Durham, 1978.

[2] J. D. Edge K. A., "The pumping dynamics of swash plate piston pumps," *Journal of Dynamic Systems, Measurement, and Control,* vol. 2, no. 111, pp. 307-312, 1989.

[3] N. D. Manring and Y. Zhang, "The improved volumetric-efficiency of an axial-piston pump utilizing a trapped-volume design," *Transactions-American Society of Mechanical Engineers Journal of Dynamic Systems Measurement and Control,* vol. 123, no. 3, pp. 479-487, 2001.

[4] G. K. a. M. I. Seeniraj, "Impact of valve plate design on noise, volumetric efficiency and control effort in an axial piston pump," in *ASME 2006 International Mechanical Engineering Congress and Exposition*, Chicago, 2006.

[5] S. Wang, "Improving the Volumetric Efficiency of the Axial Piston Pump," *Journal of Mechanical Design,* vol. 134, p. 111001, 2012.

[6] M. B. Rannow, H. C. Tu, P. Y. Li and T. R. Chase, "SOFTWARE ENABLED VARIABLE DISPLACEMENT PUMPS - EXPERIMENTAL STUDIES," in *2006 ASME International Mechanical Engineering Congress and RD&D Expo*, Chicago, Illinois, 2006.

[7] M. A. Holland, Design of digital pump/motors and experimental validation of operating strategies, PhD thesis, Purdue University, 2012.

[8] K. J. Merrill, Modeling and analysis of active valve control of a digital pump-motor, PhD diss., PURDUE UNIVERSITY, 2012.

[9] [Online]. Available: http://www.artemisip.com/our-technology.

[10] L. Wadsley, "Optimal system solutions enabled by digital pumps," in *The 52nd National Conference on Fluid Power, NCFP*, 2011.

[11] T. Royston and R. Singh, "Development of a pulse-width modulated pneumatic rotary valve for actuator position control," *Journal of dynamic systems, measurement, and control,* vol. 3, no. 115, pp. 495-505, 1993.

[12] K. Allan and J. D. Van de Ven, "Design of a high-speed on-off valve," in *ASME 2009 International Mechanical Engineering Congress and Exposition*, Lake Buena Vista, Florida, 2009..

[13] H. C. Tu, M. Rannow, J. D. Van de Ven, M. Wang, P. Li and T. Chase, "High speed rotary pulse width modulated on/off valve," in *In Proceedings of ASME-IMECE*, Seattle, 2007.

[14] B.-H. Cho, H.-W. Lee and J.-S. Oh, "Estimation technique of air content in automatic transmission fluid by measuring effective bulk modulus," *International journal of automotive technology* , vol. 2, no. 3, pp. 57-61, 2002.

[15] H. Tian and J. D. Van de Ven, "GEOMETRIC OPTIMIZATION OF A HYDRAULIC MOTOR ROTARY VALVE," in *ASME/BATH 2013 Symposium on Fluid Power & Motion Control*, Sarasota, Florida, USA, 2013.

 